







## Current vortices in aromatic carbon molecules

Thomas Stegmann <sup>1,\*</sup>, John A. Franco-Villafañe <sup>2</sup>, Yenni P. Ortiz <sup>3</sup>, Michael Deffner,<sup>4</sup> Carmen Herrmann,<sup>4</sup> Ulrich Kuhl <sup>5</sup>, Fabrice Mortessagne,<sup>5</sup> Francois Leyvraz <sup>1,6</sup> and Thomas H. Seligman <sup>1,6</sup>

<sup>1</sup>*Instituto de Ciencias Físicas, Universidad Nacional Autónoma de México, 62210 Cuernavaca, Mexico*

<sup>2</sup>*CONACYT-Instituto de Física, Universidad Autónoma de San Luis Potosí, 78290 San Luis Potosí, Mexico*

<sup>3</sup>*Instituto de Física, Universidad Nacional Autónoma de México, 04510 Mexico City, Mexico*

<sup>4</sup>*Institute for Inorganic and Applied Chemistry, University of Hamburg, 20146 Hamburg, Germany*

<sup>5</sup>*Institut de Physique de Nice, Université Côte d'Azur, CNRS, 06100 Nice, France*

<sup>6</sup>*Centro Internacional de Ciencias, 62210 Cuernavaca, Mexico*



(Received 7 May 2020; accepted 14 July 2020; published 3 August 2020)

The local current flow through three small aromatic carbon molecules, namely, benzene, naphthalene, and anthracene, is studied. Applying density functional theory and the nonequilibrium Green's function method for transport, we demonstrate that pronounced current vortices exist at certain electron energies for these molecules. The intensity of these circular currents, which appear not only at the antiresonances of the transmission but also in the vicinity of its maxima, can exceed the total current flowing through the molecular junction and generate considerable magnetic fields. The  $\pi$  electron system of the molecular junctions is emulated experimentally by a network of macroscopic microwave resonators. The local current flows in these experiments confirm the existence of current vortices as a robust property of ring structures. The circular currents can be understood in terms of a simple nearest-neighbor tight-binding Hückel model. Current vortices are caused by the interplay of the complex eigenstates of the open system which have energies close to the considered electron energy. Degeneracies, as observed in benzene and anthracene, can thus generate strong circular currents, but also nondegenerate systems like naphthalene exhibit current vortices. Small imperfections and perturbations can couple otherwise uncoupled states and induce circular currents.

DOI: [10.1103/PhysRevB.102.075405](https://doi.org/10.1103/PhysRevB.102.075405)

### I. INTRODUCTION

In the last few decades, the structural size of electronic circuits has been reduced enormously. This is manifested impressively by the fact that the first field effect transistors had the size of the palm of a hand, while nowadays, billions of transistors with size of a few nanometers are packed on a single chip. This miniaturization of electronic circuits gave rise to the question if even a single molecule can be used as the functional element of an electronic device [1] and eventually led to the founding of the active research field of molecular electronics; see, for example, Refs. [2–4] for an overview. One of the main research topics of molecular electronics is to understand the current flow through a molecular junction. A recent milestone has been the observation of quantum interference in molecular junctions [5–8] and its theoretical understanding [9–15]. However, the *local current flow*, i.e., the spatial distribution of the current in the molecule, has received less attention; see Refs. [16–46] for recent work. This can be attributed to the fact that, to the best of our knowledge, the local current flow in molecular junctions has been measured only indirectly by nuclear magnetic resonance [47,48] but not yet directly.

One remarkable theoretical prediction with respect to the local current flow is the fact that aromatic molecules can

show at certain electron energies pronounced current vortices, which can exceed even the total current flowing through the molecular junction. These predictions have been made by means of state-of-the-art theory, combining Kohn-Sham density functional theory (DFT) for the electronic structure of the molecular junction with the nonequilibrium Green's function method (NEGF) for the electron transport [20,21,39]. It has also been shown that the current vortices persist even if the molecular junction is described by a more elementary theory, namely, a tight-binding Hückel Hamiltonian, where electron-electron interactions are not taken into account, and commonly, only a single atomic orbital per atom is used [17,22–24,43,44]. Also a mixture of both approaches, the density functional based tight-binding (DFTB) method, predicts vortices in the local current flow [31]. Thermoelectric-driven ring currents were also reported recently within a tight-binding model [49]. Therefore, the observed circular currents are not a subtle many-body phenomenon but a more robust general property of ring structures. Note that vortex currents can be induced not only by an external current that is driven through the molecule but also by an external magnetic field [50–54].

In this paper, we analyze the current vortices in three small aromatic carbon molecules, namely, benzene, naphthalene, and anthracene molecules (see Fig. 1). In particular, we show that circular currents can be observed not only close to antiresonances in the transmission function but also in the vicinity of transmission maxima and hence generate

\*stegmann@icf.unam.mx

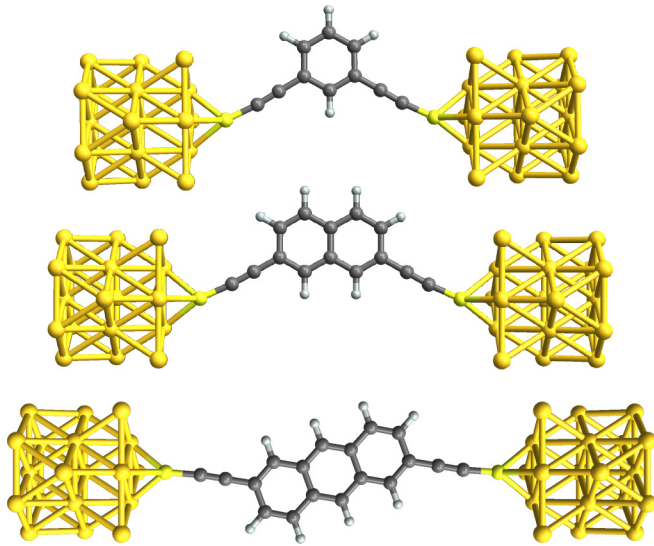


FIG. 1. Benzene (top), naphthalene (middle), and anthracene (bottom) molecules are connected via two carbon spacer atoms and a sulfur atom to gold clusters (19 atoms, fcc lattice symmetry) and hence form a molecular junction. Benzene and naphthalene are shown with leads in the meta position, while for anthracene the leads are in the para position. In our studies, both lead configurations are taken into account for all molecules.

a magnetic field. Indeed, in the following, we shall use a definition of circular current (see [22,44]) which corresponds precisely to the source of this magnetic field. More important, here we give experimental indications of current vortices in ring structures analogous to the molecular structures. The formal equivalence of the Helmholtz equation for electromagnetic waves and the noninteracting Schrödinger equation for quantum wave functions allows us to emulate quantum systems in microwave cavities [55–57]. This idea can be used to realize tight-binding systems by networks of dielectric microwave resonators [58,59] as models for graphene [60–64] and molecules [65]. Here we apply this method to emulate the current flow in aromatic carbon molecules by means of a network of dielectric resonators (see Fig. 2). By measuring the amplitude and phase of the electromagnetic field on each microwave resonator, we can investigate experimentally the local current flow in these structures. The emulation experiments clearly show circular currents as observed in the quantum calculations.

## II. SYSTEMS AND METHODS

We study the current flow in aromatic carbon molecules, benzene, naphthalene, and anthracene. These molecules are attached to gold clusters using two additional carbon spacer atoms and a sulfur atom (see Fig. 1). The gold clusters are made up of 19 atoms in the fcc lattice symmetry, although the precise configuration of the gold clusters does not qualitatively change the current flow in the molecular junction.

### A. Quantum transport calculations

In order to calculate the current flow through the molecular junction, the structure is optimized first by means of DFT as

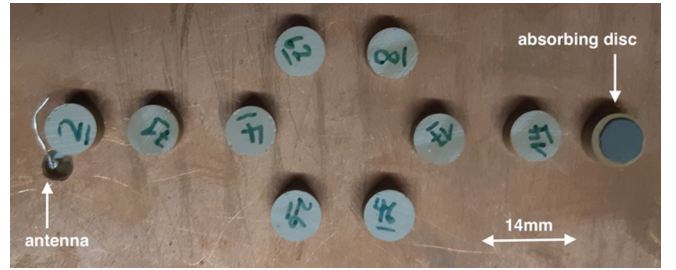


FIG. 2. Photo of the microwave emulation experiment for the benzene molecule in the para configuration of the leads. Dielectric cylindrical resonators model the carbon atoms. The source antenna, which injects microwaves, is shown on the left end. A resonator with an absorbing material glued to its top models the drain on the right end. The electromagnetic field (or wave function) is measured on each resonator by a movable antenna through the metallic top plate (not shown), which allows us to calculate the local transmissions.

implemented in the GAUSSIAN09 software package [66]. We employ standard Kohn-Sham DFT with the B3LYP exchange-correlation functional, which is a hybrid functional with 20% Hartree-Fock exchange. The LANL2MB basis set is used to describe the system. On this basis, the current flow is calculated by means of the NEGF method as implemented in the ARTAIOS software package [67]. It calculates the Green’s function of the scattering region (i.e., the molecular junction without the gold clusters)

$$G(E) = (E S - H - \Sigma_S - \Sigma_D)^{-1}, \quad (1)$$

where  $E$  is the electron energy,  $H$  is the effective single-particle Kohn-Sham Hamiltonian, and  $S$  is the overlap matrix from the DFT optimization. The self-energies  $\Sigma_{S/D}$  describe the effect of the source and drain reservoirs, which are attached through the gold clusters in order to inject and extract electrons. These reservoirs are modeled within the wideband approximation [68]. Using the Green’s function, we study the steady-state transport by means of the transmission function

$$T(E) = 4\text{Tr}[\text{Im}(\Sigma_S)G\text{Im}(\Sigma_D)G^\dagger], \quad (2)$$

as well as the local transmissions between atoms  $i$  and  $j$

$$T_{ij}(E) = \text{Im}(H_{ij}^* G_{ij}^n), \quad (3)$$

where the correlation function is given by

$$G^n = 2G\text{Im}(\Sigma_S)G^\dagger. \quad (4)$$

Note that in Eq. (3) we have assumed implicitly the sum over pairs of local basis functions which belong to the two atoms. The transmission and local transmission allow us to study the global and local transport properties of the molecular junction for electrons at energy  $E$ . In order to obtain the current from the transmission and the local transmissions, one has to integrate these functions within the bias voltage window. Also note that the stability of qualitative conclusions on conductance and transport pathways with respect to varying the approximate exchange-correlation functional was studied before, e.g., in Ref. [21], and was found to be negligible. Details of the methods can be found in Refs. [4,69–72].

### B. Microwave emulation experiments

In the following we show that a tight-binding-Hückel model of a quantum system can be emulated efficiently by coupled dielectric resonators with a high index of refraction sandwiched between two metallic plates [62,73] (see Fig. 2). The steady-state transport of electrons of energy  $E$  through the system is emulated by microwaves of frequency  $\nu$ .

Let us define the  $z$  axis to be perpendicular to the metallic plates. Due to the (approximate) cylindrical symmetry, the solution can be separated in cylindrical coordinates. The first transverse electric (TE) mode has only one nonvanishing magnetic component,  $B_z$ , which factorizes in a  $z$ -dependent sinusoidal part and a radially symmetric dependence on  $x$  and  $y$ . Thus, the whole vectorial problem has been reduced to a scalar description, where the value of  $B_z$  at the center of the resonator corresponds to the single-electron wave function. It is important to note here that the microwave experiment does not mimic any electron-electron interaction. The dielectric resonators have high-quality TE resonances, which are excited by a linear dipolar antenna (source antenna) and a loop antenna (movable antenna), both parallel to the plane of the metallic plates. As the first TE resonance of the dielectric resonator is below the cutoff frequency of the free propagation in air, the field outside the resonators is rapidly decaying in the air between the metal plates. Due to the high quality factors of the resonators (TEMEX 2000 series,  $Q \approx 2000$ ) and the strongly decaying coupling, the magnetic field inside the resonators is practically not affected by the presence of the other resonators once placed sufficiently far apart. This guarantees the validity of a tight-binding description for the experiment once the appropriate couplings and eigenfrequencies are used. In contrast to molecular systems the couplings in the microwave experiment are positive, and thus, the eigenfrequency of the symmetric and antisymmetric eigenmodes are interchanged. Hence, we have found an experimental setup that emulates the single-electron tight-binding Hückel model [74,75]. For more details on the experimental background, refer to [62,76]. This setup was successfully used to emulate graphenelike structures [60,61,63,64] and the transport through polyacetylene chains [65].

Here we use this technique to gain insight into the local current flow in aromatic carbon molecules. The carbon atoms are represented by identical cylindrical resonators (5 mm high, 4 mm in radius, refractive index  $n \approx 6$ ). The nearest-neighbor distance of the resonators is, on average, 14 mm, while their precise distance ratios reflect the interatomic distances found by the DFT optimization of the molecule. The coupling strength between neighboring resonators decays approximately exponentially, as shown previously [62,65]. Such an exponential decay is a realistic model for slightly varying carbon-carbon bond distances, as shown for deformed graphene [77]. The hydrogen atoms are not taken into account explicitly, as we assume that the current is carried predominantly by the  $\pi$  electron system that is formed by the  $2p_z$  orbitals of the carbon atoms. These orbitals, as well as their interactions, are emulated by the microwave resonator network.

The effects of the gold clusters and sulfur atoms are taken into account indirectly by the antenna on the left end that

injects microwaves and a resonator with an absorbing material glued to its top on the right end which serves as the drain. The microwaves are injected as transverse electrical modes around the frequency  $\nu_0 = 6.65$  GHz, where the individual resonators have an isolated resonance. Note that in contrast to the theory, the source (injecting antenna) and drain (absorbing resonator) are modeled differently in the emulation experiment (compare Figs. 1 and 2). The other components of the molecular junction (gold, sulfur, and hydrogen atoms), their complicated interactions, and correlations between the electrons are taken into account (approximately) in the DFT-NEGF calculations but not in the emulation experiments. To what extent molecules composed of different types of atoms can be modeled by means of different types of microwave resonators will be addressed in future work.

In order to determine the local transmission in the resonator network, the electromagnetic field (or wave function)  $\psi(\mathbf{r})$  is measured on each resonator by means of a movable antenna through the metallic top plate. The probability current density

$$\mathbf{j}(\mathbf{r}) = \frac{\hbar}{m} \text{Im}[\psi^*(\mathbf{r})\nabla\psi(\mathbf{r})] \quad (5)$$

has a one-to-one correspondence to the Poynting vector in a cylindrical microwave cavity setup [78,79]. By discretizing it, we obtain, for the transmission between two resonators at frequency  $\nu$ ,

$$T_{ij}^{\text{mw}}(\nu) = \text{Im}(d_{ij}^{-1} \psi_i^* \psi_j), \quad (6)$$

where  $d_{ij}$  is the distance between resonators  $i$  and  $j$ . Note that in the case of a noninteracting system, Eq. (6) is formally equivalent to Eq. (3) because  $G_{ij}^n \sim \psi_i^* \psi_j$  and  $d_{ij}$  is proportional to the coupling matrix elements  $H_{ij}$  [69,70].

## III. RESULTS AND DISCUSSION

### A. Benzene

Let us begin our discussion with the simplest aromatic carbon molecule, namely, benzene. The transmission calculated by means of the DFT-NEGF method is shown in Fig. 3 (top) for the para and meta configurations of the leads. In both configurations, transmission band gaps, resonances, and antiresonances can be observed. Instead of the global transport properties of the molecular junction, which were addressed previously [4], we rather investigate here on which pathways the current flows through the system. Typical transmission pathways, which can be observed by varying the electron energy, are shown in Fig. 4 by means of arrows of different sizes and color shading. Note that these local transmissions are normalized with respect to the maximum value at each electron energy (or microwave frequency) and hence do not reflect the absolute transmission through the molecule. Moreover, transmissions less than 10% of the maximal value are not plotted.

Starting with the para configuration, we observe that the normalized transmission pathways are independent of the electron energy and split up into two paths that carry equal amounts of current. These properties can be understood easily by the mirror symmetry of the molecular junction with respect to the horizontal axis through the center of the carbon

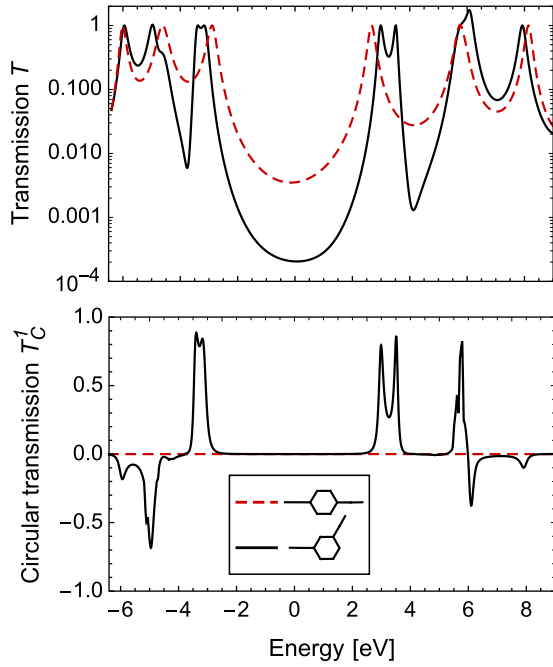


FIG. 3. Calculated transmission  $T$  (top) and circular transmission  $T_C^1$  [bottom, calculated by Eq. (7)] in the benzene molecule with leads in the meta (black curve) and para (red dashed curve) configurations. The transmission shows in both cases band gaps, resonances, and antiresonances. Note that the middle between the HOMO and LUMO resonance energies has been chosen to be the origin of the energy scale. Strong circular currents can be observed for certain electron energies in the meta configuration, while in the para configuration no current vortices exist.

hexagon, which implicates identical currents in both paths, and hence, circular currents are not possible.

In the meta configuration, we observe that within the transmission band gap ( $E \sim 0$  eV), the current is flowing on the shortest path between the source and drain. Such asymmetric transmission pathways are possible as the molecular junction is no longer mirror symmetric with respect to the horizontal axis. If we change the electron energy to the transmission resonances, we observe a circular current that is rotating around the carbon ring. Passing through the antiresonance (at  $E \sim 4$  eV), the direction of rotation changes. The full dependence of the transmission pathways on the electron energy (or microwave frequency) is shown in three movies in the Supplemental Material [80–82].

The circular transmission pathways in the carbon hexagon  $\alpha$  are quantified by [22,44]

$$T_C^\alpha(E) = \frac{1}{L_\alpha} \sum_{\substack{i,j \in \alpha \\ i < j}} T_{ij}(E) \operatorname{sgn}[(\mathbf{r}_i - \mathbf{r}_\alpha) \times (\mathbf{r}_j - \mathbf{r}_\alpha)], \quad (7)$$

where  $T_{ij}(E)$  is the local transmission between two carbon atoms located at positions  $\mathbf{r}_i$  and  $\mathbf{r}_j$ . The sum is over all atoms which are part of the hexagon  $\alpha$  with center  $\mathbf{r}_\alpha$  and length  $L_\alpha$ . The circular transmission as a function of the electron energy is shown in Fig. 3 (bottom). The circular transmission, calculated in terms of the normalized transmissions, is indicated in Fig. 4 by the color shading of the carbon hexagons. Both

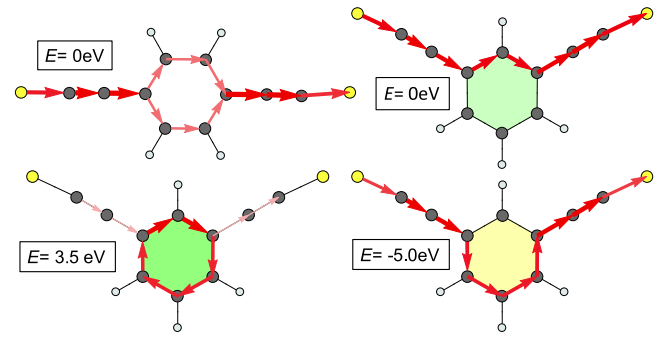


FIG. 4. Normalized transmission pathways (arrows) in the benzene molecular junction, calculated by the DFT-NEGf method. The carbon, hydrogen, and sulfur atoms are represented by dark gray, light gray, and yellow disks, respectively. The gold clusters (see Fig. 1) are not shown. The size and color shading of the arrows indicate the magnitude of the local transmissions. The color shading of the hexagons indicates the normalized circular transmissions  $T_C^1$  [see Eq. (7)]; greenish colors indicate clockwise circulation, and yellowish colors show the opposite direction. For the above-shown transmission pathways the full dependence on the electron energy is shown as a movie in the Supplemental Material [80].

Figs. 3 and 4 confirm the existence of circular currents in meta-benzene for certain energies ranges, whereas no current vortices exist in para-benzene.

The circular transmissions give rise to a magnetic field passing through the carbon rings. In order to estimate its strength, we integrate  $T_C^1(E)$  around the double resonance at 3 eV within a bias window of 2 eV (to be precise, in the energy range from 2 to 4 eV) and obtain an absolute circular current of approximately  $I_C \sim 30 \mu\text{A}$ , which in turn causes in the center of the carbon hexagon a magnetic field of  $B \sim 150$  mT.<sup>1</sup> This value should be considered only a rough estimate of the generated magnetic field because a simple approach for the spatial distribution of the local current is used here (i.e., it is assumed that the current flows on the direct path between two atoms). Note that the circular transmission in Eq. (7) is defined in such a way that it is the only source of magnetic field that passes through the ring. In other words, the remaining transverse current does not generate any magnetic flux; see Refs. [22,44] for details. Transmission pathways like those at  $E = 0$  eV and  $E = -5$  eV are also considered to be current vortices because they have a finite circular transmission and give rise to a magnetic field. However, this magnetic field will be weaker and more inhomogeneous than in the cases where the current is circulating unidirectionally around the complete carbon ring like at  $E = 3.5$  eV.

Now, let us turn to the data from the microwave emulation experiment. Figure 5 shows the transmission  $T$  and circular transmission  $T_C^1$  as a function of the microwave frequency as well as the (normalized) transmission pathways

<sup>1</sup>The magnetic field on an axis, which goes perpendicular through the center of a carbon hexagon, is given by  $B(z) = \frac{3\sqrt{3}\mu_0 I_C}{4\pi a} \frac{1}{[(z/a)^2 + 3/4]\sqrt{(z/a)^2 + 1}}$ , where  $a \sim 0.139$  nm is the distance of the carbon atoms and  $I_C$  is the current circulating in the hexagon.

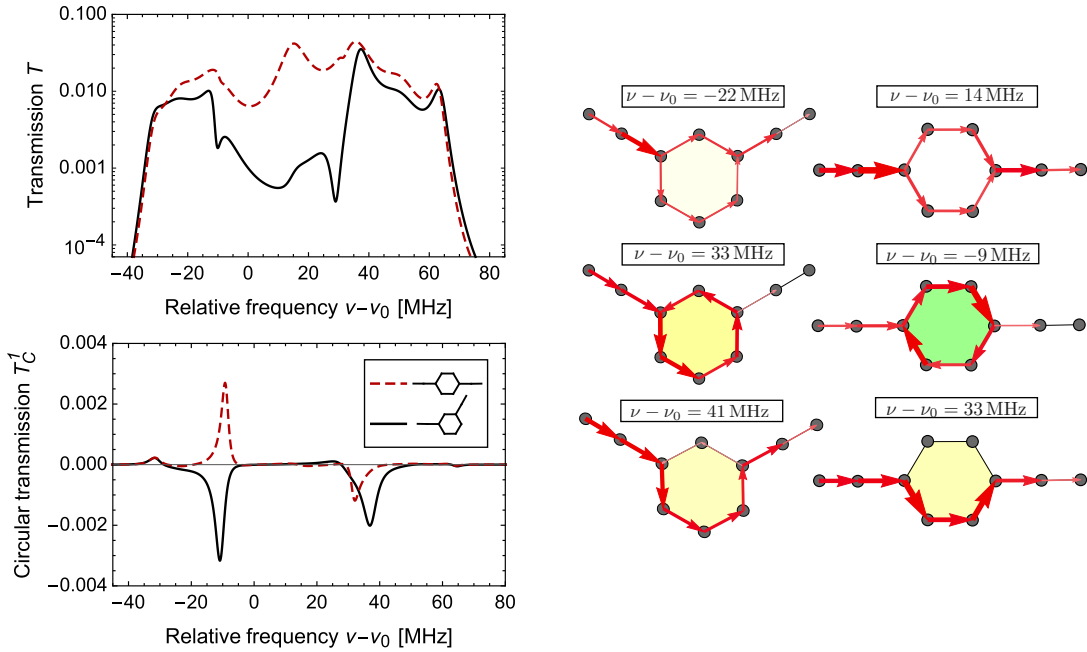


FIG. 5. Current flow in the microwave emulation experiment. Left: Transmission and circular transmission as a function of the microwave frequency. Right: Normalized transmission pathways at different microwave frequencies. The microwave experiment clearly confirms the existence of circular currents. The transmission pathways as a function of the microwave frequency can be found as a movie in the Supplemental Material [81].

for various microwave frequencies. The transmission shows several resonances and antiresonances, similar to the DFT-NEGF calculations. However, their number differs because the microwave experiment emulates only the noninteracting  $\pi$  electron system, while in the DFT-NEGF calculations all electrons are taken into account. The emulation experiment shows a considerable reduction of the transmission (in the range from  $-10$  to  $30$  MHz) in the meta configuration, which resembles the band gap observed in the DFT-NEGF calculations. In the para configuration, the transmission is rather constant, while the DFT-NEGF calculations show a (less pronounced) band gap. This discrepancy can be explained again by the fact that only part of the electronic structure is emulated by the experiment because the simple tight-binding model discussed below shows trends similar to the emulation experiment (see Fig. 7). Moreover, the overall transmission is lower, and its features are much less pronounced than in the calculations, which can be explained by the overall absorption of the microwaves [64,65]. Note that the transmission is measured between the antenna on the left end (see Fig. 2) and the antenna on top of the next-to-last site on the right end. If the antenna is placed on top of the last site on the right end, the transmission that passes through the absorber is measured. It follows the same trends as the transmission to the next-to-last site but is damped strongly (approximately one order of magnitude).

The transmission pathways in the meta-benzene analog show strong circular currents at certain frequencies and agree qualitatively with the patterns obtained in the DFT-NEGF study, although a sign reversal of the circular transmission is not found. In para-benzene, we find transmission pathways that are similar to the theoretical predictions, but surprisingly, we also observe asymmetric patterns as well as current vortices. Note that in both cases the local transmissions are

not conserved due to the absorption of the microwaves. In particular, the transmissions towards the drain at the right end decay strongly because of the absorber on top of the last resonator, which damps the current that is passing to the measuring antenna (on top of this resonator).

In order to better understand the observed effects, let us consider a simple nearest-neighbor tight-binding model for the benzene molecule. The Hamiltonian, its eigenenergies, and its eigenstates are shown in Fig. 6. By means of these eigenstates, we can calculate the current that is flowing in the isolated molecule (i.e., in the absence of the leads) at the corresponding eigenenergies. The nondegenerate states at  $E = \pm 2$  do not cause any current flow because they are entirely real. The degenerate states at  $E = \pm 1$  are complex valued and generate nonzero ring currents with opposite directions of rotation. The same observation holds for the angular

$$H^{\text{tb}} = \begin{pmatrix} 0 & 1 & 0 & 0 & 0 & 1 \\ 1 & 0 & 1 & 0 & 0 & 0 \\ 0 & 1 & 0 & 1 & 0 & 0 \\ 0 & 0 & 1 & 0 & 1 & 0 \\ 0 & 0 & 0 & 1 & 0 & 1 \\ 1 & 0 & 0 & 0 & 1 & 0 \end{pmatrix}$$

$E$   
 $2$   
 $1$   
 $0$   
 $-1$   
 $-2$

$\psi_2 = e^{2\pi i p}$   
 $\psi_1^\pm = e^{\pm i\pi/3 p}$   
 $\psi_{-1}^\pm = e^{\pm i2\pi/3 p}$   
 $\psi_{-2} = e^{i\pi p}$

FIG. 6. Left: Nearest-neighbor tight-binding model of benzene. Right: Eigenenergies and eigenstates. The variable  $p \in (0, 1, 2, 3, 4, 5)$  numerates cyclically the six carbon atoms and generates the six components of the eigenstates.

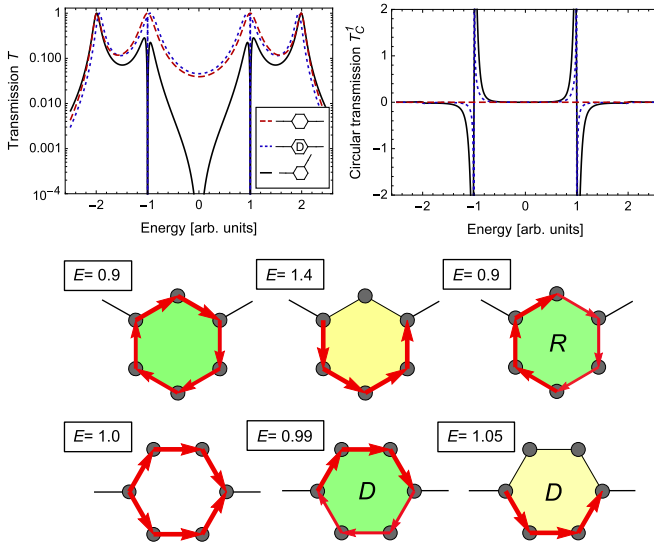


FIG. 7. Current flow in the benzene molecule modeled by a simple tight-binding Hamiltonian (Fig. 6) and wideband leads [Eq. (8)]. The transmission and circular transmission (top) show features similar to the microwave emulation experiment. The transmission pathways (bottom) show vortices that are obtained also in the DFT-NEGF calculations and the experiment. The pathway with the label *R* has been obtained by taking into account only the two eigenstates close to  $E = 1$ . For the pathways with the label *D*, we have introduced random fluctuations (5%) in the coupling energies, which induces circular currents. The full dependence of the transmission pathways as a function of the electron energy can be found as a movie in the Supplemental Material [82].

momentum of these states as it is proportional to the circular current in Eq. (7) [22,44].<sup>2</sup> However, note that one could choose the degenerate eigenstates also in such a way that their ring currents and angular momenta are zero.

The coupling of the molecule to the leads is modeled within the wideband approximation with the self-energy matrix elements

$$\Sigma_{ij}^{S/D} = -i\eta\delta_{i,j}\delta_{i,s/d}, \quad (8)$$

where  $s = 1$  is the position of the source, while  $d = 4$  and  $d = 3$  give the position of the drain in the para and meta configurations, respectively. The parameter  $\eta = 0.2$  controls the coupling strength of the leads, and  $\delta_{ij}$  is the Kronecker delta function. On the one hand, this non-Hermitian perturbation of the system lifts the degeneracies of the eigenstates, but on the other hand, all of these eigenstates have zero angular momentum. However, the transmission pathways calculated by means of Eq. (3) agree qualitatively with the DFT-NEGF calculations and the microwave experiment and confirm the existence of circular currents (see Fig. 7). The transmission

<sup>2</sup>The expected value of the angular momentum of a tight-binding state  $\psi$  is determined by  $\langle\psi|L|\psi\rangle \sim \sum_{i<j} \text{Im}(H_{ij}^* \psi_i^* \psi_j) [(\mathbf{r}_i - \mathbf{r}_0) \times (\mathbf{r}_j - \mathbf{r}_0)]$ , where  $\mathbf{r}_i$  are the positions of the sites (or atoms) with respect to the center  $\mathbf{r}_0$ . The angular momentum is proportional to the circular current in Eq. (7) because  $G_{ij}^n \sim \psi_i^* \psi_j$ .

in the tight-binding model shows several resonances like in the DFT-NEGF calculation, but their total number is lower because the tight-binding Hamiltonian takes into account only the  $\pi$  orbitals of the carbon atoms, while in the DFT-NEGF calculation the full electronic structure, including the  $\sigma$  system, is taken into account, which can lead to more resonances. An analytic study of the benzene molecular junction that focuses on quantum interference can be found in Ref. [83].

To understand the existence of these vortices, we expand the local transmission (3) in terms of the eigenstates of the open system  $H + \Sigma_S + \Sigma_D$ . As the open system is non-Hermitian, we have a set of right eigenstates  $\psi_\alpha$  and left eigenstates  $\tilde{\psi}_\alpha$ , which are related here by complex conjugation,  $\tilde{\psi}_\alpha = \psi_\alpha^*$ . Using the completeness of the set of eigenfunctions, we obtain the spectral representation of the Green's function matrix elements [4],

$$G_{ij}(E) = \sum_{\alpha} \frac{\psi_{\alpha,i} \psi_{\alpha,j}}{E - \varepsilon_{\alpha}}, \quad (9)$$

where  $\varepsilon_{\alpha}$  are the complex eigenenergies of the open system. Taking into account the particular form of the self-energies (8), we obtain finally, for the local transmission,

$$T_{ij}(E) = 2\eta \sum_{\alpha,\beta} \text{Im} \left[ H_{ij}^* \frac{\psi_{\alpha,s} \psi_{\alpha,i} \psi_{\beta,j}^* \psi_{\beta,s}^*}{(E - \varepsilon_{\alpha})(E - \varepsilon_{\beta}^*)} \right]. \quad (10)$$

Let us start with the meta configuration. Taking into account in the sum in Eq. (10) only the two eigenstates close to  $E = \pm 1$ , which are degenerate in the absence of the leads, we observe qualitatively the same circular transmission pathways (see in Fig. 7 the benzene molecule marked *R*). Taking into account in Eq. (10) only the diagonal terms (i.e.,  $\alpha = \beta$ ) or considering only one of the two eigenstates gives qualitatively different (and hence incorrect) transmission pathways without any ring currents. In para benzene, where ring currents are not possible due to the symmetry of the molecular junction (see above), one of the degenerate eigenstates at  $E = \pm 1$  (i.e., the state  $\psi'_{\pm 1} = \psi_{\pm 1}^+ - \psi_{\pm 1}^-$ ) is unchanged by the leads because it has zero value on the carbon atoms where the leads are attached. This eigenstate does not couple to the leads and does not contribute to the current flow. The current around  $E = \pm 1$  is determined by a single eigenstate and does not show any vortices. The reader maybe interested in a discussion of related problems using molecular orbitals in Ref. [36]. Note that the above discussion focuses on those vortices which can unambiguously be assigned to one specific pair of degenerate states. Vortex currents also exist for energies far from such degenerate pairs, but they are significantly lower; see our discussion on naphthalene below.

The fact that the microwave experiment shows circular currents also in the para configuration of the benzene molecule can be explained by the imperfections of the experiment. The resonance frequency of the dielectric resonators ( $\pm 5$  MHz) and their position ( $\pm 0.2$  mm) vary slightly due to manufacturing imperfections and limited precision in placing them, respectively. We take into account these imperfections in the tight-binding calculations by changing randomly the nearest-neighbor coupling energies by 5%. This induces circular currents also in para benzene (see the transmission pathways with the label *D* in Fig. 7). In terms of Eq. (10), the random

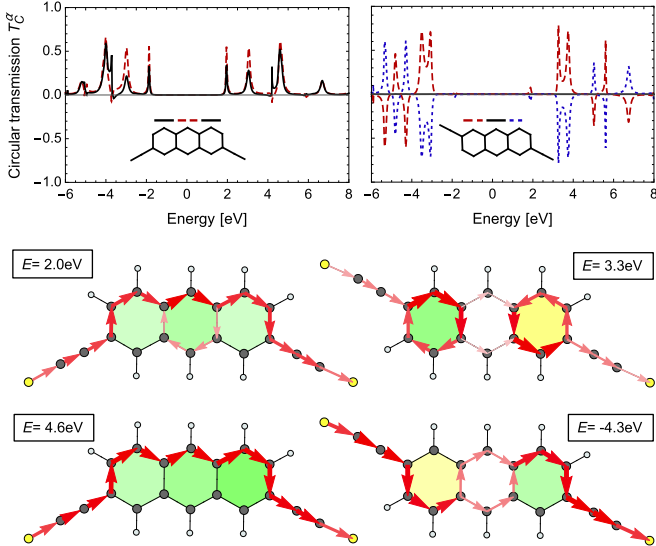


FIG. 8. Current flow in the anthracene molecular junction calculated by means of the DFT-NEGF method. The meta configuration is shown in the left column; the para configuration is shown in the right column. Top: Circular transmission in the three  $[\alpha \in (1, 2, 3)]$  carbon rings. Bottom: Transmission pathways at various electron energies.

perturbations couple the (previously uncoupled) eigenstates  $\psi'_{\pm 1}$  to the leads and hence induce current vortices. As the perturbations are small, the coupling is weak, and ring currents are observed only in a narrow window around  $E = \pm 1$ . Taking into account this type of disorder in the meta configuration does not change qualitatively the observed current patterns because *a priori* all eigenstates are coupled to the leads.

### B. Anthracene and naphthalene

Now, let us proceed with longer carbon ring molecules, namely, anthracene and naphthalene. The circular transmission and the transmission pathways, calculated by the DFT-NEGF method, are shown in Fig. 8 for the meta and para configurations of the anthracene molecular junction. The corresponding results from the microwave emulation experiment are shown in Fig. 9. Theory and experiment confirm the existence of circular currents for the two configurations of the leads.

The circular currents can be understood by a simple tight-binding Hamiltonian, similar to our discussion of the benzene molecule (see Fig. 6). In anthracene, we have four twofold-degenerate eigenstates at the energies  $E = \pm 1$  and  $E = \pm\sqrt{2}$ , where strong current vortices can appear (see Fig. 10). Let us consider a pair of these degenerate states. When the leads are attached to the molecule, the degeneracy is lifted, but only in the para configuration do both states couple to the leads. Taking into account in Eq. (10) only these two states shows that they determine the transmission pathways in the proximity of their eigenenergy. In particular, the correlations between the states, taken into account in Eq. (10) by the elements with  $\alpha \neq \beta$ , contribute significantly to the current flow. When the leads are attached in the meta position, one of the previously degenerate states has zeros at the positions

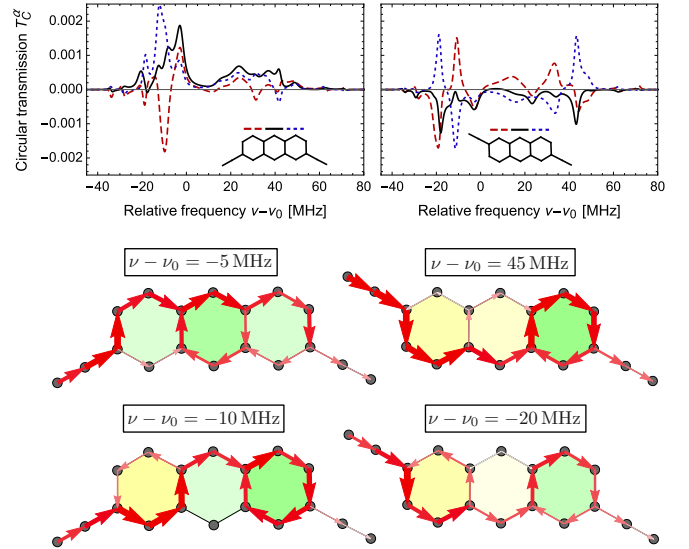


FIG. 9. Circular transmission (top) and transmission pathways (bottom) obtained by the microwave emulation experiment of the anthracene molecule. Current vortices are observed in both configurations of the leads.

of the source and drain and hence does not couple to them. The fact that circular transmission pathways are found in meta anthracene can be explained by the interplay of states that are nondegenerate in the isolated molecule but close in energy. This also explains why the circular transmissions are much less pronounced in this configuration of the leads.

In the calculation, the local transmissions and the circular transmission in the three carbon rings show certain symmetries. For example, in the meta configuration the circular transmissions in the first and third carbon rings are equal,  $T_C^1 = T_C^3$ , while in the para configuration they have opposite signs,  $T_C^1 = -T_C^3$ , and they have zero value in the central ring  $T_C^2 = 0$ . These symmetries cannot be observed in the microwave experiment due to the different modeling of the

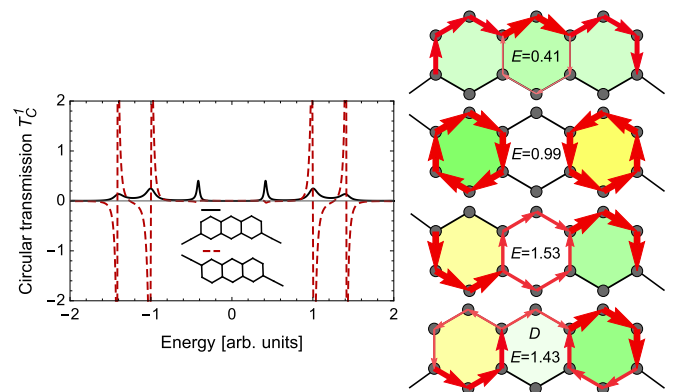


FIG. 10. Circular transmission (left) and transmission pathways (right) in the anthracene molecular junction, calculated within a simple nearest-neighbor tight-binding model. The transmission pathways agree qualitatively with the DFT-NEGF calculations and the microwave experiment. The asymmetric transmission pathway labeled *D* is obtained by changing randomly the coupling energies by 5%.

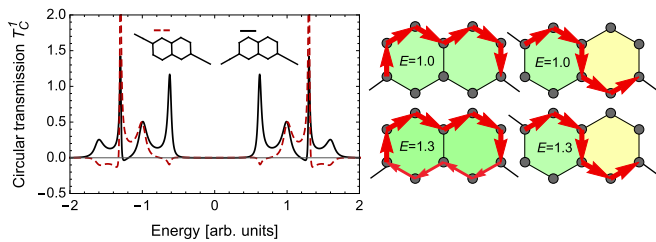


FIG. 11. Circular transmission (left) and transmission pathways (right) in the naphthalene molecular junction, calculated within a simple nearest-neighbor tight-binding model. Although all eigenstates of the isolated molecule are nondegenerate, the open system shows circular currents.

source and drain and the imperfections of the experiment (see above). Randomly changing the coupling energies by 5% in the tight-binding model, we obtain asymmetric current patterns very similar to those obtained in the emulation experiment (see, for example, in Fig. 10 the transmission pathway labeled *D*).

Finally, we address briefly the naphthalene molecule, using a simple tight-binding model. All eigenstates of this molecule are nondegenerate and real. No degenerate pairs as in the case of benzene and thus no vortex currents that become exceptionally large at specific energies exist. However, when leads are coupled to the molecule and transport is studied, circular transmission pathways are observed, see Fig. 11, but their shape differs from the pathways found in benzene and anthracene because they are global ring currents that extend over the whole molecule. In general, they are a consequence of the interplay of all eigenstates of the open system [see Eq. (10)], where the main contributions come from the eigenstates that are close to the considered energy.

#### IV. CONCLUSIONS AND OUTLOOK

We have presented an analysis of the local current flow in benzene and anthracene with some remarks on naphthalene. We have performed state-of-the-art DFT-NEGF calculations of the current flow as well as microwave emulation experiments that model the noninteracting  $\pi$  electron system of the molecule. Both show qualitatively similar transmission pathways and confirm the existence of current vortices in certain regions of electron energies (see, for example, Figs. 3–5). These experiments prove the existence of circular currents in macroscopic ring structures that emulate a tight-binding quantum model of the carbon molecules. The circular currents can be understood in terms of a simple nearest-

neighbor tight-binding Hückel model which also connects more deeply the DFT-NEGF calculations and the emulation experiments, as it approximates the former and describes qualitatively the latter.

Using the spectral decomposition of the local transmissions [see Eq. (10)], we have shown that the circular currents can be understood by the interplay of the complex eigenstates with energies close to the considered electron energy. In particular, the cross terms ( $\alpha \neq \beta$ ) have a significant effect. Degenerate states, as they appear in benzene and anthracene, generate strong circular currents if both states couple to the leads (like in meta-benzene). One of these states alone cannot induce a current vortex. We have also shown that small imperfections and perturbations can couple previously uncoupled states to the leads and hence induce current vortices in the system even if symmetry conditions forbid, at first, their occurrence (see Fig. 7).

As to the significance of the results we can only speculate, but practical use may result from the magnetic field caused by vortices of strong circular transmission. These vortices appear close to transmission maxima and tend to show currents circulating around the complete ring, which imply stronger and more homogeneous magnetic fields within the ring than currents flowing on only one side of the ring. A main challenge to detecting this magnetic field is not only to realize experimentally the molecular junctions but also to shift the Fermi energy close to one of the resonances of the circular transmission [84]. We plan to investigate if this can be achieved by designing specific aromatic molecules, for example, by adding substituents [85] or by changing the molecular structure [86]. We also expect that current vortices will appear in larger aromatic carbon molecules, like graphene nanoribbons, which may be easier to implement in the experiment. Our findings may pave the way for molecular generators and detectors of magnetic fields. They may also help to control and engineer precisely the local current flow in nanoelectronic devices.

#### ACKNOWLEDGMENTS

We gratefully acknowledge funding from CONACYT Proyecto Fronteras 952, Proyecto A1-S-13469, Proyecto A1-S-18696, UNAM-PAPIIT Projects IA101618, IA103020, AG100819, DFG Project HE 5675/5-1, and EU Project NEMF21. Y.P.O. is grateful for an UNAM-DGAPA postdoctoral fellowship. We acknowledge use of the MIZTLI supercomputing facility of DGTIC-UNAM. We thank R. Garcia for computer technical support and T. Stuyver for his help with the ARTAIOS code.

- [1] A. Aviram and M. A. Ratner, *Chem. Phys. Lett.* **29**, 277 (1974).
- [2] A. Nitzan and M. Ratner, *Science* **300**, 1384 (2003).
- [3] *Introducing Molecular Electronics*, edited by G. Cuniberti and G. R. K. Fagas (Springer, Berlin, 2005).
- [4] J. C. Cuevas and E. Scheer, *Molecular Electronics* (World Scientific, Singapore, 2017).
- [5] C. M. Guédon, H. Valkenier, T. Markussen, K. S. Thygesen, J. C. Hummelen, and S. J. van der Molen, *Nat. Nanotechnol.* **7**, 305 (2012).

- [6] D. Z. Manrique, C. Huang, M. Baghernejad, X. Zhao, O. A. Al-Owaedi, H. Sadeghi, V. Kalignedji, W. Hong, M. Gulcur, T. Wandlowski *et al.*, *Nat. Commun.* **6**, 6389 (2015).
- [7] M. Carloti, A. Kovalchuk, T. Wächter, X. Qiu, M. Zhamnikov, and R. C. Chiechi, *Nat. Commun.* **7**, 13904 (2016).
- [8] Y. Li, M. Buerkle, G. Li, A. Rostamian, H. Wang, Z. Wang, D. R. Bowler, T. Miyazaki, L. Xiang, Y. Asai *et al.*, *Nat. Mater.* **18**, 357 (2019).



- [9] G. C. Solomon, D. Q. Andrews, T. Hansen, R. H. Goldsmith, M. R. Wasielewski, R. P. V. Duyne, and M. A. Ratner, *J. Chem. Phys.* **129**, 054701 (2008).
- [10] T. Markussen, R. Stadler, and K. S. Thygesen, *Nano Lett.* **10**, 4260 (2010).
- [11] M. Berritta, D. Z. Manrique, and C. J. Lambert, *Nanoscale* **7**, 1096 (2015).
- [12] S. Sangtarash, H. Sadeghi, and C. J. Lambert, *Nanoscale* **8**, 13199 (2016).
- [13] X. F. Yang, Y. W. Kuang, Y. S. Liu, D. B. Zhang, Z. G. Shao, H. L. Yu, X. K. Hong, J. F. Feng, X. S. Chen, and X. F. Wang, *Nanoscale* **8**, 15712 (2016).
- [14] D. Nozaki and C. Toher, *J. Phys. Chem. C* **121**, 11739 (2017).
- [15] L. Ulčakar, T. Rejec, J. Kokalj, S. Sangtarash, H. Sadeghi, A. Ramšak, J. H. Jefferson, and C. J. Lambert, *Sci. Rep.* **9**, 3478 (2019).
- [16] Y. Xue and M. A. Ratner, *Phys. Rev. B* **70**, 081404(R) (2004).
- [17] M. Ernzerhof, H. Bahmann, F. Goyer, M. Zhuang, and P. Rocheleau, *J. Chem. Theory Comput.* **2**, 1291 (2006).
- [18] N. Sai, N. Bushong, R. Hatcher, and M. Di Ventra, *Phys. Rev. B* **75**, 115410 (2007).
- [19] P. Fowler, N. Mizoguchi, D. Bean, and R. Havenith, *Chem. Eur. J.* **15**, 6964 (2009).
- [20] G. C. Solomon, C. Herrmann, T. Hansen, V. Mujica, and M. A. Ratner, *Nat. Chem.* **2**, 223 (2010).
- [21] C. Herrmann, G. C. Solomon, and M. A. Ratner, *J. Phys. Chem. C* **114**, 20813 (2010).
- [22] D. Rai, O. Hod, and A. Nitzan, *J. Phys. Chem. C* **114**, 20583 (2010).
- [23] D. Rai, O. Hod, and A. Nitzan, *Phys. Rev. B* **85**, 155440 (2012).
- [24] S. K. Maiti, *Eur. Phys. J. B* **86**, 296 (2013).
- [25] D. A. Bahamon, Z. Qi, H. S. Park, V. M. Pereira, and D. K. Campbell, *Nanoscale* **7**, 15300 (2015).
- [26] F. Al-Dirini, M. A. Mohammed, M. S. Hossain, F. M. Hossain, A. Nirmalathas, and E. Skaftidas, *Nanoscale* **8**, 10066 (2016).
- [27] P. Lazzaretto, *Phys. Chem. Chem. Phys.* **18**, 11765 (2016).
- [28] G. Monaco and R. Zanasi, *Phys. Chem. Chem. Phys.* **18**, 11800 (2016).
- [29] D. Sundholm, R. J. F. Berger, and H. Fliegl, *Phys. Chem. Chem. Phys.* **18**, 15934 (2016).
- [30] M. Dimitrova, H. Fliegl, and D. Sundholm, *Phys. Chem. Chem. Phys.* **19**, 20213 (2017).
- [31] D. Nozaki and W. G. Schmidt, *J. Comput. Chem.* **38**, 1685 (2017).
- [32] H. Li, M. H. Garner, T. A. Su, A. Jensen, M. S. Inkpen, M. L. Steigerwald, L. Venkataraman, G. C. Solomon, and C. Nuckolls, *J. Am. Chem. Soc.* **139**, 10212 (2017).
- [33] T. Hansen, G. C. Solomon, and T. Hansen, *J. Chem. Phys.* **146**, 092322 (2017).
- [34] T. Stuyver, N. Blotwijk, S. Fias, P. Geerlings, and F. De Proft, *ChemPhysChem* **18**, 3012 (2017).
- [35] S. Fias and T. Stuyver, *J. Chem. Phys.* **147**, 184102 (2017).
- [36] S.-M. Jhan and B.-Y. Jin, *J. Chem. Phys.* **147**, 194106 (2017).
- [37] T. Stuyver, S. Fias, P. Geerlings, F. D. Proft, and M. Alonso, *J. Phys. Chem. C* **122**, 19842 (2018).
- [38] V. Pohl, L. E. M. Steinkasserer, and J. C. Tremblay, *J. Phys. Chem. Lett.* **10**, 5387 (2019).
- [39] G. Cabra, A. Jensen, and M. Galperin, *J. Chem. Phys.* **148**, 204103 (2018).
- [40] M. H. Garner, H. Li, Y. Chen, T. A. Su, Z. Shanguan, D. W. Paley, T. Liu, F. Ng, H. Li, S. Xiao *et al.*, *Nature (London)* **558**, 415 (2018).
- [41] A. Jensen, M. H. Garner, and G. C. Solomon, *J. Phys. Chem. C* **123**, 12042 (2019).
- [42] M. H. Garner, A. Jensen, L. O. H. Hyllested, and G. C. Solomon, *Chem. Sci.* **10**, 4598 (2019).
- [43] M. Patra and S. K. Maiti, *Sci. Rep.* **7**, 43343 (2017).
- [44] U. Dhakal and D. Rai, *J. Phys.: Condens. Matter* **31**, 125302 (2019).
- [45] A. Taninaka, S. Yoshida, Y. Sugita, O. Takeuchi, and H. Shigekawa, *Nanoscale* **11**, 5951 (2019).
- [46] Z.-Q. Zhang, J.-T. Lü, and J.-S. Wang, *Phys. Rev. B* **101**, 161406(R) (2020).
- [47] A. Troisi and M. A. Ratner, *Phys. Chem. Chem. Phys.* **9**, 2421 (2007).
- [48] A. Troisi, J. M. Beebe, L. B. Picraux, R. D. van Zee, D. R. Stewart, M. A. Ratner, and J. G. Kushmerick, *Proc. Natl. Acad. Sci. USA* **104**, 14255 (2007).
- [49] J. B. Rix and P. Hedegård, *J. Phys. Chem. C* **123**, 3817 (2019).
- [50] G. Merino, T. Heine, and G. Seifert, *Chem. Eur. J.* **10**, 4367 (2004).
- [51] R. Islas, T. Heine, and G. Merino, *Acc. Chem. Res.* **45**, 215 (2011).
- [52] H. Fliegl, S. Taubert, O. Lehtonen, and D. Sundholm, *Phys. Chem. Chem. Phys.* **13**, 20500 (2011).
- [53] D. Sundholm, H. Fliegl, and R. J. Berger, *Wiley Interdiscip. Rev.: Comput. Mol. Sci.* **6**, 639 (2016).
- [54] R. Báez-Grez, L. Ruiz, R. Pino-Rios, and W. Tiznado, *RSC Adv.* **8**, 13446 (2018).
- [55] H.-J. Stöckmann, *Quantum Chaos* (Cambridge University Press, Cambridge, 1999).
- [56] U. Kuhl, H.-J. Stöckmann, and R. Weaver, *J. Phys. A* **38**, 10433 (2005).
- [57] D. Laurent, O. Legrand, P. Sebbah, C. Vanneste, and F. Mortessagne, *Phys. Rev. Lett.* **99**, 253902 (2007).
- [58] J. A. Franco-Villafañe, E. Sadurní, S. Barkhofen, U. Kuhl, F. Mortessagne, and T. H. Seligman, *Phys. Rev. Lett.* **111**, 170405 (2013).
- [59] C. Poli, M. Bellec, U. Kuhl, F. Mortessagne, and H. Schomerus, *Nat. Commun.* **6**, 6710 (2015).
- [60] U. Kuhl, S. Barkhofen, T. Tudorovskiy, H.-J. Stöckmann, T. Hossain, L. de Forges de Parivy, and F. Mortessagne, *Phys. Rev. B* **82**, 094308 (2010).
- [61] M. Bellec, U. Kuhl, G. Montambaux, and F. Mortessagne, *Phys. Rev. Lett.* **110**, 033902 (2013).
- [62] M. Bellec, U. Kuhl, G. Montambaux, and F. Mortessagne, *Phys. Rev. B* **88**, 115437 (2013).
- [63] J. Böhm, M. Bellec, F. Mortessagne, U. Kuhl, S. Barkhofen, S. Gehler, H.-J. Stöckmann, I. Foulger, S. Gnuzmann, and G. Tanner, *Phys. Rev. Lett.* **114**, 110501 (2015).
- [64] T. Stegmann, J. A. Franco-Villafañe, U. Kuhl, F. Mortessagne, and T. H. Seligman, *Phys. Rev. B* **95**, 035413 (2017).
- [65] T. Stegmann, J. A. Franco-Villafañe, Y. P. Ortiz, U. Kuhl, F. Mortessagne, and T. H. Seligman, *Phys. Lett. A* **381**, 24 (2017).
- [66] M. J. Frisch *et al.*, Gaussian 09, Revision A.02, Gaussian Inc., Wallingford (USA), 2016.
- [67] M. Deffner, L. Groß, T. Steenbock, B. A. Voigt, G. C. Solomon, and C. Herrmann, ARTAIOS, a code for postprocessing quantum

- chemical electronic structure calculations, <https://www.chemie.uni-hamburg.de/institute/ac/arbeitsgruppen/herrmann/software/artaios.html>.
- [68] C. J. O. Verzijl, J. S. Seldenthuis, and J. M. Thijssen, *J. Chem. Phys.* **138**, 094102 (2013).
- [69] S. Datta, *Electronic Transport in Mesoscopic Systems* (Cambridge University Press, Cambridge, 1997).
- [70] S. Datta, *Quantum Transport: Atom to Transistor* (Cambridge University Press, Cambridge, 2005).
- [71] A. Pecchia and A. D. Carlo, *Rep. Prog. Phys.* **67**, 1497 (2004).
- [72] C. Herrmann, G. C. Solomon, J. E. Subotnik, V. Mujica, and M. A. Ratner, *J. Chem. Phys.* **132**, 024103 (2010).
- [73] S. Barkhofen, M. Bellec, U. Kuhl, and F. Mortessagne, *Phys. Rev. B* **87**, 035101 (2013).
- [74] E. Hückel, *Z. Phys.* **70**, 204 (1931).
- [75] E. Hückel, *Z. Phys.* **72**, 310 (1931).
- [76] M. Reisner, F. Mortessagne, E. Makri, T. Kottos, and U. Kuhl, *Acta Phys. Pol. A* **136**, 790 (2019).
- [77] R. M. Ribeiro, V. M. Pereira, N. M. R. Peres, P. R. Briddon, and A. H. Castro Neto, *New J. Phys.* **11**, 115002 (2009).
- [78] P. Seba, U. Kuhl, M. Barth, and H.-J. Stöckmann, *J. Phys. A* **32**, 8225 (1999).
- [79] M. Barth and H.-J. Stöckmann, *Phys. Rev. E* **65**, 066208 (2002).
- [80] See Supplemental Material at <http://link.aps.org/supplemental/10.1103/PhysRevB.102.075405> for a movie which shows the transmission pathways in the benzene molecular junction as a function of the electron energy, calculated by the DFT-NEGF method.
- [81] See Supplemental Material at <http://link.aps.org/supplemental/10.1103/PhysRevB.102.075405> for a movie which shows the transmission pathways in the emulation experiment as a function of the microwave frequency.
- [82] See Supplemental Material at <http://link.aps.org/supplemental/10.1103/PhysRevB.102.075405> for a movie which shows the transmission pathways in the benzene molecular junction as a function of the electron energy, calculated within a simple tight-binding model.
- [83] T. Hansen, G. C. Solomon, D. Q. Andrews, and M. A. Ratner, *J. Chem. Phys.* **131**, 194704 (2009).
- [84] X. Liu, S. Sangtarash, D. Reber, D. Zhang, H. Sadeghi, J. Shi, Z.-Y. Xiao, W. Hong, C. J. Lambert, and S.-X. Liu, *Angew. Chem. Int. Ed.* **56**, 173 (2016).
- [85] C. Herrmann, G. C. Solomon, and M. A. Ratner, *J. Am. Chem. Soc.* **132**, 3682 (2010).
- [86] H. Schlicke and C. Herrmann, *ChemPhysChem* **15**, 4011 (2014).